Australian Journal of Earth Sciences

An International Geoscience Journal of the Geological Society of Australia

ISSN: (Print) (Online) Journal homepage: https://www.tandfonline.com/loi/taje20

Quartz oxygen isotopes from Tick Hill area in Mount Isa Inlier: indication of a regional fluid overprint

T. X. Le, P. H. G. M. Dirks, I. V. Sanislav, C. Harris, J. M. Huizenga, H. A. Cocker & G. N. Manestar

AUSTRALIAN JOURNAL OF EARTH SCIENCES
https://doi.org/10.1080/08120099.2022.1985608

Quartz oxygen isotopes from Tick Hill area in Mount Isa Inlier: indication of a regional fluid overprint

T. X. Le[a,b], P. H. G. M. Dirks[a], I. V. Sanislav[a], C. Harris[c], J. M. Huizenga[a,d,e], H. A. Cocker[a] and G. N. Manestar[a]

[a]EGRU (Economic Geology Research Centre), College of Science and Engineering, James Cook University, Townsville, Australia; [b]Faculty of Geosciences and Geology Engineering, Hanoi University of Mining and Geology, Hanoi, Vietnam; [c]Department of Geological Sciences, University of Cape Town, Rondebosch, South Africa; [d]Faculty of Environmental Sciences and Natural Resource Management, Norwegian University of Life Sciences, Ås, Norway; [e]Department of Geology, University of Johannesburg, Johannesburg, South Africa

ABSTRACT

At the Tick Hill gold deposit, $\delta^{18}O_{quartz}$ data for the mineralised lithologies and surrounding rocks are similar and fall within a narrow range of 10.5–13.7‰ V-SMOW. The highly mineralised quartzo-feldspathic mylonite has quartz $\delta^{18}O$ ($\delta^{18}O_{quartz}$) values of 11.3–13.6‰, which are similar to values for the surrounding rocks both locally and regionally, *i.e.* $\delta^{18}O_{quartz}$ by itself does not provide a useful exploration tool. The $\delta^{18}O_{quartz}$ values from the Tick Hill area most likely reflect the late Isan hydrothermal overprint at 1525–1520 Ma. The origin of the altering fluids is unclear, as the $\delta^{18}O_{quartz}$ values overlap with reported $\delta^{18}O$ values calculated for both metamorphic and igneous fluids. When combining the $\delta^{18}O_{quartz}$ results with $\delta^{18}O_{calcite}$ results available from the literature, a temperature of 350–550 °C was calculated, which is consistent with observed alteration assemblages associated with gold mineralisation.

ARTICLE HISTORY
Received 25 June 2021
Accepted 22 September 2021

KEYWORDS
oxygen isotope; Mount Isa; Mary Kathleen; Tick Hill; gold deposit; Isan Orogeny

KEY POINTS

1. The $\delta^{18}O_{quartz}$ values (10.5–13.7‰ V-SMOW) of Au-rich quartz–feldspar mylonite are indistinguishable from the altered host rocks both local and regional.
2. The narrow range of $\delta^{18}O_{quartz}$ values for the rock units in the Tick Hill area and Mary Kathleen Domain most likely reflect a regional fluid overprint.
3. The post-mineralised quartz–calcite veins yield higher $\delta^{18}O_{quartz}$ values (14.1–17‰), possibly reflecting (partial) re-equilibration of minerals locally formed in late cataclastic fault rocks.

Introduction

The Tick Hill deposit is a unique high-grade deposit in the Mount Isa Inlier (Figure 1) with abundant pure free gold and minor sulfide and carbonate alteration. The carbonate veins that occur in association with the ore body are texturally late and not associated with the main stages of mineralisation (Le *et al.*, 2021a). Gold mineralisation is concentrated along a highly strained shear zone between hanging-wall and footwall quartzite units and is characterised by partly annealed, $D_{1–2}$, blasto-mylonite that formed in quartz–feldspar and calcsilicate gneiss, and biotite schist. The mineralised mylonite is associated with intense D_3 silicification, which involved pervasive silica alteration as well as the emplacement of numerous, thin quartz veins both parallel to and at high angles to the mylonitic layering. Apart from quartz veining, D_3 alteration was also associated with the emplacement of quartz–feldspar veins with extensive metasomatic haloes and pegmatite veins (Le *et al.*, 2021a).

Gold at Tick Hill occurs towards the centre of a strongly silicified zone and gold grains are commonly hosted within or intergrown with quartz that is distributed along the main mylonitic fabric. The paucity of sulfide and carbonate minerals in association with high-grade gold mineralisation is a challenge for conducting a systematic S or C–O isotope study of the Tick Hill deposit. Instead, we focused on the collection of $\delta^{18}O$ values for quartz grains from rocks associated with the deposit, in line with earlier studies at Tick Hill (Choy, 1994; Hannan, 1994).

Oxygen isotope values for quartz can provide information on the source(s) of fluids (Faure, 1986; Kleine *et al.*, 2018). During the exploration stage, $\delta^{18}O_{quartz}$ studies at Tick Hill (Choy, 1994; Hannan, 1994) mostly focused on quartzite units and quartz veins that were linked to gold mineralisation but did not include the dominant rock types in the Au-rich units (*i.e.* quartz–feldspar mylonite and intensely silicified units) or many of the common rock types in the area (*e.g.* syn- and post-tectonic intrusions,

CONTACT T. X. Le truong.le@my.jcu.edu.au EGRU James Cook University Townsville, Townsville, QLD 4811, Australia
Editorial handling: Anita Andrew

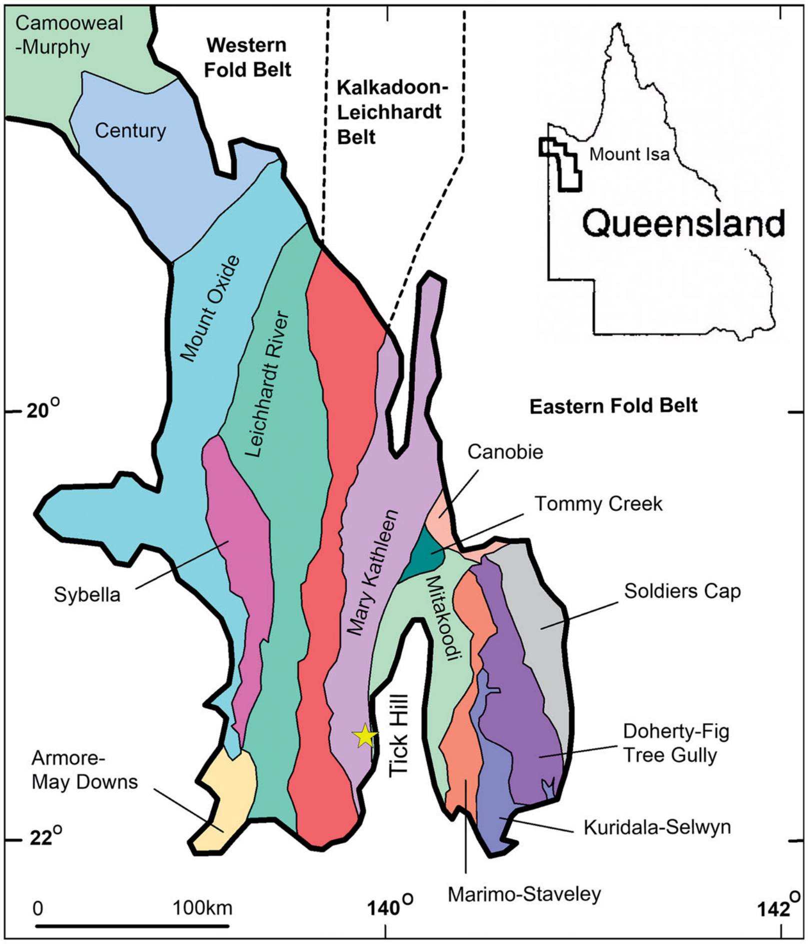

Figure 1. Tectonic subdivisions in the Mount Isa Inlier (adapted from Blake, 1987; Withnall & Hutton, 2013).

calcsilicate, amphibolite, late quartz veins). Quartzite ridges, like the hanging-wall quartzite, were interpreted as silicified D_1 shear zones and conduits for mineralising fluids suggesting the $\delta^{18}O$ values of quartz from these shears could be used in exploration (*e.g.* Hannan, 1994). The $\delta^{18}O$ values reported in this study include quartz selected from Au-rich quartz–feldspar mylonite and a variety of other rock types that occur in the immediate vicinity of the deposit. The aims of the study are: (1) to assess the oxygen isotope data obtained during earlier studies; (2) to determine if the highly mineralised zones are characterised by specific $\delta^{18}O_{quartz}$ values that are distinct from less altered distal host rocks; (3) to ascertain whether significant differences exist between similar rock types of different ages (*i.e.* compare $\delta^{18}O_{quartz}$ results for early-, syn- and late- tectonic rocks); and (4) to explain the $\delta^{18}O$ values in Au-bearing quartz.

Geological background

Regional geology

The Tick Hill deposit is situated in the southern part of the Mary Kathleen Domain (MKD) in the Eastern Fold Belt, Mount Isa Inlier (Figure 1). The inlier preserves igneous and Paleo- to Meso-Proterozoic tectono-stratigraphic sequences that formed during 1890–1500 Ma, in a series of successive geological events. The Mount Isa Inlier is subdivided into three north-trending tectonic domains (Blake, 1987; Withnall & Hutton, 2013): the Western Fold Belt, the Kalkadoon-Leichhardt Belt and the Eastern Fold Belt (EFB; Figure 1).

The earliest volcano-sedimentary sequences in the inlier (1890–1870 Ma; Foster & Austin, 2008; Withnall & Hutton, 2013) were metamorphosed to amphibolite facies during the 1870–1840 Ma Barramundi Orogeny (Blake, 1987; Withnall & Hutton, 2013). Following the Barramundi Orogeny, sedimentary and volcanic rocks were deposited during three periods of basin formation (Giles *et al.*, 2002) described in the literature either as cover sequences (Blake, 1987; Blake & Steward, 1992) or more recently as superbasins (*i.e.* Leichhardt, Calvert and Isan superbasins; Gibson *et al.*, 2016). In this contribution, we use the superbasin terminology. The Leichhardt Superbasin sequences were deposited during 1790–1740 Ma and this period of deposition was interrupted by the 1740–1710 Ma Wonga and Burstal magmatic events and the associated deformation and metamorphism (Foster & Austin, 2008; Kositcin *et al.*, 2019; Le *et al*., 2021b; Neumann *et al*., 2009; Spence *et al*., 2021; Withnall & Hutton, 2013). The Calvert Superbasin sequences were deposited during 1730–1640 Ma, whereas the Isan Superbasin sequences were deposited during 1640–1580 Ma. Between 1670 and 1650 Ma, the Sybella batholith intruded in the western part of the inlier whereas a series of smaller intrusive bodies, which include the Tommy Creek granite and the Ernest Henry diorite, intrude the eastern part of the inlier (*e.g.* Foster & Austin, 2008; Pollard & McNaughton, 1997).

The tectonic activity culminated with the prolonged, 1650–1500 Ma, Isan Orogeny (*e.g.* Betts *et al*., 2006; MacCready *et al*., 2006), which variably affected the entire inlier and reached peak-metamorphic conditions between 1600 and 1580 Ma (*e.g.* Abu Sharib & Sanislav, 2013; Foster & Rubenach, 2006). The Williams and Naraku batholiths (Blake & Steward, 1992; Page & Sun, 1998) were emplaced between 1550 and 1490 Ma, during the final stages of the Isan Orogeny. Mafic dykes are a ubiquitous component of the Mount Isa Inlier and range in age from pre-Barramundi to 1100 Ma (Blake & Steward, 1992).

The metamorphic and deformational history of the MKD is complex and involves a series of deformation and intrusive events that appear to be diachronous along the belt. For example, in the southern part of the MKD, the 1790–1770 Ma granites intrude deformed metasediments suggesting that this part of the domain experienced an earlier tectonic history compared with rocks further north (Le *et al*., 2021b). The remainder of the MKD appears to have a consistent deformation history synchronous with the emplacement of the Wonga-Burstall plutons between 1750 and 1710 Ma (*e.g.* Holcombe *et al*., 1991; Le *et al*., 2021b; Oliver, 1995; Passchier & Williams, 1989; Spence *et al*., 2021). The MKD was variably overprinted by the Isan Orogeny (*e.g.* Le *et al*., 2021b; Oliver, 1995; Spence *et al*., 2021).

Local geology

The Tick Hill deposit is located in the southern part of MKD (Figure 1). The deposit is hosted by a sequence comprising calcsilicate gneiss, amphibolite, biotite schist, quartzite, and quartz–feldspar mylonite that was intruded by a series of 1780–1770 Ma granitic plutons (Figure 2; Le *et al*., 2021b). At least four deformation events have been recognised based on field and overprinting relationships (Le *et al*., 2021a). The earliest deformation event, D_1, produced an intense, layer parallel schistosity (gneissic layering in granitic sills and some calcsilicates) with a well-developed mineral lineation that was folded during D_2 around upright, tight folds with a steep, north–south-trending axial plane. The D_3 deformation consists of a series of north- to north-east-trending fault zones with a brittle–ductile character and shear sense indicators suggesting normal movement. The D_4 deformation consists of steeply north-dipping brittle faults recording mainly strike-slip movement and overprinting earlier structures.

The D_{1-2} deformation occurred during peak-metamorphic conditions estimated at 6.0–7.6 kbar (garnet–plagioclase–hornblende–quartz barometry; Le, 2021) and 720–760 °C (hornblende–plagioclase thermometry; Le, 2021). Actinolite alteration and chlorite thermometry indicate that D_3 deformation occurred over a wide range of temperatures (130–550 °C; Le, 2021). The D_4 structures are characterised by cataclasite and fault gauge comprising quartz, calcite, host-rock fragments and clay minerals, collectively indicating low temperatures at shallow crustal conditions. The timing of D_{1-2} deformation was constrained between 1790 and 1770 Ma based on U–Pb zircon ages of syn-tectonic (*i.e.* syn-D_{1-2}) granites, whereas the timing of D_3 deformation was constrained at 1525–1520 Ma based on U–Pb zircon ages from syn-D_3 pegmatites (Le *et al*., 2021b).

Gold mineralisation at Tick Hill formed during two discrete events, syn-D_1 and syn-D_3. Early gold grains and inclusions intergrown with syn-D_1 peak-metamorphic minerals (*i.e.* diopside, scapolite and hornblende) indicate gold accumulation during D_1 (Le *et al*., 2021a). This mineralisation episode involved silicification and the formation of magnetite concentrated in the hanging wall of the orebody. The second stage of gold mineralisation is hosted by D_3 fractures and associated alteration that overprints earlier quartz–feldspar mylonite and intensely silicified units (Le *et al*., 2021a). The alteration associated with syn-D_3 mineralisation includes: (1) the destruction of magnetite; (2) the emplacement of abundant laminar quartz veins resulting from quartz–feldspar alteration overprinting the D_{1-2} mylonitic rocks; and (3) the formation of proximal albite, hematite, chlorite, actinolite, epidote overprinted by later K-feldspar, sericite, clay minerals and minor calcite. The presence of selenides in the ore assemblage suggests low pressure conditions (<1 kbar; Le *et al*., 2021a).

Historical oxygen isotope studies

In an MSc thesis study of the Tick Hill deposit (Choy, 1994), nine $\delta^{18}O_{quartz}$, six $\delta^{18}O_{whole\ rock}$, two $\delta^{18}O_{magnetite}$ values and one $\delta^{18}O_{albite}$ value for samples from drill holes TH034 and TH076 (Table 1) were reported, with individual samples subdivided into peak-metamorphic, syn-D_1 samples and late-tectonic syn-D_3 samples. The sample descriptions are cursory, and all samples were allocated to D_1 but are clearly affected by D_3 alteration, thus casting doubt on the validity of the D_1–D_3 classification. Choy (1994) reported that the mineralised quartz–feldspar mylonite has a $\delta^{18}O_{whole\ rock}$ value of 11.2‰. However, based on the sample description, the other two quartz vein samples associated with gold mineralisation could be interpreted to be associated with mineralised quartz–feldspar mylonite. Thus, the mineralised quartz–feldspar mylonite in Choy (1994) has an average $\delta^{18}O_{whole\ rock}$ value of 12.3 ± 0.3‰ (n = 3). Quartz from the altered calcsilicate rock in the immediate hanging wall of the deposit has a similar average $\delta^{18}O_{quartz}$ value of 12.3 ± 0.7‰ (n = 6). Choy (1994) linked these

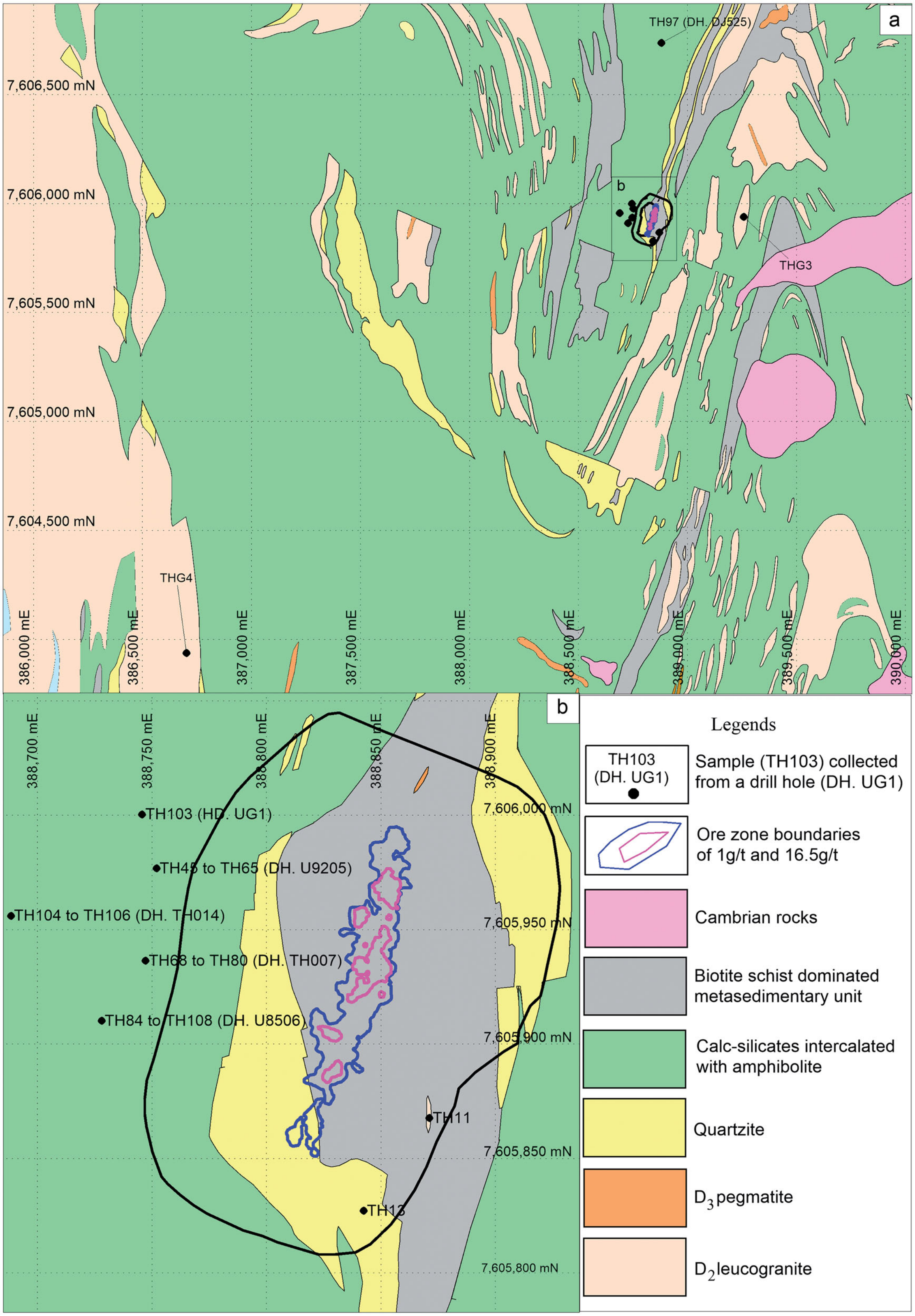

Figure 2. Locations of samples used in quartz oxygen isotope studies at Tick Hill. (a) Regional geological map and (b) enlargement in Tick Hill mine area. The datum is Zone 54-GDA94.

results to a granite intrusion-derived fluid that affected the quartz–feldspar mylonite but provided little evidence in support of this interpretation.

As part of an exploration targeting exercise, Hannan (1994) reported $\delta^{18}O_{quartz}$ data for samples collected by Boda (1994). Samples analysed were mainly from quartzite

Table 1. $\delta^{18}O$ values for samples from Tick Hill reported by Choy (1994).

No.	Sample ID	Rock type	Mineral	$\delta^{18}O$ (‰) V-SMOW	Timing	Description
1	76–150.15W	Quartz–feldspar mylonite	Whole rock	11.2	D_1	Whole rock (quartz–feldspar mylonite)
2	34–208.25	Quartz vein	Quartz	12.0	D_3	Vein quartz, 14 m above Au zone
3	34–264.7Q	Quartz vein/quartz–feldspar mylonite?	Quartz	13.2	D_3	Quartz, from quartz vein, with sericitised plagioclase, chlorite and scapolite
4	76–176.2	Quartz vein	Quartz	11.7	D_3	From quartz in quartz vein in plagioclase–epidote
5	34–242.1	Quartz vein/quartz–feldspar mylonite?	Quartz	12.6	D_1	Clean quartz from quartz vein; with apatite and trace Au
6	34–234	Quartz vein	Quartz	12.4	D_1	Clean quartz from quartz vein; 7 m above the ore zone
7	34–264.7B	Wall-rock schist (calcsilicate?)	Quartz	11.7	D_1	Quartz, from wall rock
8	76–148.7	Wall rock, schist	Quartz	12.3	D_1	Hand-picked quartz from wall rock in gold-bearing zone
9	76–150.32	Wall rock, schist (calcsilicate)	Quartz	12.9	D_1	Hand-picked quartz (plagioclase–amphibole–chlorite–epidote schist)
10	76–152.8W	Wall rock (calcsilicate)	Whole rock	11.9	D_3	Whole rock (scapolite–amphibole schist, with sericitised scapolite and iron oxide-stained amphibole)
11	34–267.1W	Wall rock schist (calcsilicate)	Whole rock	9.3	D_1	Wall rock (scapolite–biotite–amphibole schist)
12	34–280W	Wall rock, schist (meta-pelite)	Whole rock	11.0	D_1	Whole rock (biotite–sillimanite–plagioclase–albite schist)
13	76–155W	Wall rock, schist (calcsilicate)	Whole rock	11.9	D_1	Whole rock (scapolite–amphibole–quartz rock)
14	76–171W	Wall rock?/altered granite?	Whole rock	9.0	D_1	Whole rock (plagioclase–biotite–albite schist)
15	34–221.55	Wall rock, schist	Magnetite	3.7	D_1	Hand pick magnetite in calcsilicate rocks above the ore zone
16	76–144.85	No information	Magnetite	11.6	D_1	Hand-picked magnetite
17	76–150.15Q	No information	Quartz	11.8	D_1	Quartz separate
18	34–220.7	No information	Albite	7.3	D_3	Albite separate

Rock type descriptions and structural timing are based on original descriptions by Choy (1994). Note the D_1 and D_3 in Choy (1994) equal to D_{1-2} and late D_3, respectively, of this study.

ridges and associated laminar quartz ribbons in the mineralised mylonite zones (Table 2). Hannan (1994) interpreted the quartz ridges as silicified D_1 decollement zones that he expected would have a depleted $\delta^{18}O$ signature compared with regional values. For 13 quartz samples, he reported an average $\delta^{18}O_{quartz}$ value of 12.0 ± 0.6‰, with little variation as a function of rock type or sample location (*i.e.* structural position). Hannan (1994) noted a depleted $\delta^{18}O_{quartz}$ value of 10.3‰ for one gold-bearing quartz laminate sample interpreted to be the main D_1 decollement zone and proposed testing depleted $\delta^{18}O_{quartz}$ values to identify D_1 shear zones. He concluded that the narrow range of $\delta^{18}O_{quartz}$ values for quartz in the mine and the wider district indicates equilibration of the country rocks with a single fluid within a narrow temperature range and attributed this to the presence of a homogenous fluid at high metamorphic grade. The quartzites in the region do not have $\delta^{18}O_{quartz}$ values that differentiate them from other rocks in the region.

Regional $\delta^{18}O_{calcite}$ values for the MKD and interpretation of potential fluid sources were presented in Oliver (1995) and Oliver *et al.* (1993). Oliver *et al.* (1993) provided a large dataset for $\delta^{13}C$ and $\delta^{18}O$ values from calcite pods and surrounding calcsilicate rocks and meta-dolerite in the Corella Formation along the length of the MKD between Mt Godkin in the north and the Trekelano mine in the south. The calcite pods are associated with albite–titanite–pargasite/actinolite–diopside (±chalcopyrite–pyrrhotite) alteration and were interpreted to be emplaced immediately after peak metamorphism, during or immediately after D_2 with the formation of upright folds at metamorphic conditions of 530–570 °C (calcite–dolomite geothermometry). Oliver *et al.* (1993) interpreted this as occurring at *ca* 1550 Ma under calculated regional peak-metamorphic conditions of 530–630 °C and 3–4 kbar for the area under investigation. The retrograde (*i.e.* syn-D_3) veins, which were interpreted to form a continuum with D_2 veins, occurred in similar structural positions to the earlier veins but are mineralised and associated with retrograde greenschist–amphibolite facies assemblages. Oliver *et al.* (1993) also sampled late (*i.e.* D_4) quartz–calcite veins associated with the large quartz veins and breccia zones along faults, such as the Fountain Range Fault in the central MKD. The $\delta^{18}O_{calcite}$ values for the calcite pods, and adjacent altered calcsilicate and meta-dolerite wall-rock samples, were similar along the length of the MKD and varied between 10.5 and 12.5‰ (with $\delta^{13}C_{calcite}$ ranging from −7 to −2‰ V-PDB). Away from the calcite pods, meta-dolerite wall-rock samples have $\delta^{18}O_{whole\text{-}rock}$ values of 3.5–7.0‰, and unaltered calcsilicate and marble with enriched $\delta^{18}O_{calcite}$ values of 18–21‰ (with $\delta^{13}C_{calcite}$ ranging from −1.6 to −0.6‰), which were interpreted to be representative of calcite $\delta^{13}C$ and $\delta^{18}O$ values for regional unaltered calcsilicate rock. The $\delta^{18}O_{calcite}$ results did not vary as a function of host-rock type, meaning that the isotope values are not a result of mixing with locally derived fluids and

Table 2. $\delta^{18}O_{quartz}$ values for samples from Tick Hill area as reported by Hannan (1994).

No.	Sample ID	Rock type	$\delta^{18}O$‰ V-SMOW	Description
1	MQ41066	Quartz–feldspar mylonite	11.3	Ore-lode horizon with ribbon quartz, underground mining
2	MQ41072	Quartz–feldspar mylonite	10.3	Underground mining, no information of Au
3	MQ41061	Quartzite	12.3	Foot wall quartzite, 100 m N of the open pit
4	MQ41063	Quartzite	12.5	Hanging wall quartzite, 100 m N of the open pit
5	MQ41065	Quartzite	12.2	Hanging wall quartzite, pit wall
6	MQ41064	Quartzite	11.9	Hanging wall quartzite, 800 m S of the open pit
7	MQ41067	Quartzite	11.7	At Surveyor's Hill
8	MQ41068	Quartzite	12.9	At Petticoat Creek, west ridge
9	MQ41070	Quartz ridge	12.2	Quartz ridge, 2.5 km south Tick Hill
10	MQ41071	Quartz ridge	12.4	Quartz ridge, 2.5 km south Tick Hill
11	MQ41065a	Wall rock	12.1	Underground mine
12	MQ41062	Wall rock	11.7	Amphibole-rich wall rock, 100 m N of the open pit
13	MQ41069	Granofels	12.5	At Petticoat Creek, west ridge

were not in isotopic equilibrium with the immediate host rocks. Rather, the homogenous $\delta^{18}O_{calcite}$ values were the result of infiltration of isotopically homogenous fluids not derived from the Corella Formation exposed on the surface today. The $\delta^{18}O_{calcite}$ values for D_4 veins were similar to the values from the older veins. Oliver (1995) and Oliver *et al.* (1993) speculated that the ultimate source of the fluids could be crystallising magma in the lower crust or upper mantle, and possibly linked to intrusions at depth linked like the extensive granite in the eastern Mount Isa Inlier. The local variation in isotopic values is explained by the minor component contributed by devolatilisation reactions in the calcsilicate and marble units (Oliver *et al.*, 1993).

Methodology

A total of 39 quartz samples from different rock types at Tick Hill selected for this study are described in Table 3 and their locations shown in Figure 2. The samples include 18 specimens of mineralised quartz–feldspar mylonite, with quartz obtained from either the mylonite fabric, or from thin quartz veins or lamellae emplaced parallel to the mylonitic fabric that locally resemble ribbon grains (*e.g.* Figure 3a–f). Two samples of non-gold-bearing, D_3 quartz–feldspar veins that overprint the intensely silicified units were taken to compare with those from the Au-bearing samples (*e.g.* Figure 3g, h). Five quartz samples were taken from intensely silicified and locally mineralised amphibole-rich calcsilicate within the ore zone, or in the immediate hanging wall (*e.g.* Figure 4a, b) together with a footwall quartzite and two hanging-wall quartzite samples (*e.g.* Figure 4c, d). Seven samples were collected from D_3 pegmatite veins or quartz–feldspar veins, and two samples were collected from post-mineralisation (D_4) quartz and quartz–carbonate veins (*e.g.* Figure 4e–g). Lastly, quartz from three D_2 leucogranite samples was collected for this study (*e.g.* Figure 4h).

Samples were crushed into sand-sized grains before being panned, sieved and cleaned in distilled water. After drying, 30–40 g of quartz grains was hand-picked under the microscope; for the Au-rich samples, Au-bearing quartz grains were preferentially selected. The samples were analysed at the University of Cape Town, South Africa, by laser fluorination. Approximately 1–3 mg of quartz (1–5 grains) per sample was analysed. Quartz grains were loaded into a polished Ni sample holder placed in the oven at 110 °C for at least 1 h before being transferred to the reaction chamber. After pumping for over 2 h, the BrF_5 at 10 kPa was released into the reaction chamber for 30 seconds and left overnight to react with the quartz. After the reaction was completed, excess BrF_5 and free Br were frozen into a cold finger, while the remained gas was passed through a KCl trap at ~200 °C to remove any F_2. Sample gas was expanded into a double-U trap in liquid nitrogen, and the purified O_2 was collected in a molecular sieve set in glass bottles. A blank sample was run daily to check there was no contribution to O_2 from leaks in the system. The long-term difference in pairs of the MONGT in-house standard analysed with each batch of samples (2008–2020) is 0.12 ($n = 341$, $2\sigma = 0.16$). The details of the technique have been described in Harris and Vogeli (2010). Oxygen isotopic ratios are reported relative to V-SMOW in per mille (‰)

Results

The $\delta^{18}O_{quartz}$ values for the 39 samples (Table 3) are plotted with $\delta^{18}O_{quartz}$ data from previous studies by Choy (1994), Hannan (1994) and Oliver *et al.* (1993) in Figure 5. Most (*i.e.* 34 of the 39 samples) of the $\delta^{18}O_{quartz}$ results from the different rock types are between 10.5 and 13.6‰. The $\delta^{18}O_{quartz}$ values for Au-rich, syn-tectonic (D_{1-2}), quartz–feldspar mylonite mainly vary between 11.3 and 13.6‰ ($n = 16$, average value of 12.4 ± 0.7‰) with two outliers of 14.9 and 15.3‰. Samples of D_3 quartz–feldspar veins overprinting the intensely silicified D_1 mylonitic texture has similar $\delta^{18}O_{quartz}$ values of 11.9 and 12.8‰ (Table 3). The intensely silicified amphibolitic unit that occurs in close association with the mineralisation has $\delta^{18}O_{quartz}$ values of 12.2 to 13.1‰ ($n = 4$, average value of 12.5 ± 0.4‰), with a distinct outlier of 19.4‰. The $\delta^{18}O_{quartz}$ results for syn-D_2 leucogranites in the Tick Hill area (including samples THG3 and THG4, which were dated at 1778 ± 10 Ma and 1777 ± 10 Ma, respectively; Le *et al.*, 2021b) are 11.2 and 11.8‰, respectively, *i.e.* similar to the mineralised quartz–feldspar mylonite from the pit (Le *et al.*, 2021b). The $\delta^{18}O_{quartz}$ values for the D_3 hydrothermal quartz–feldspar

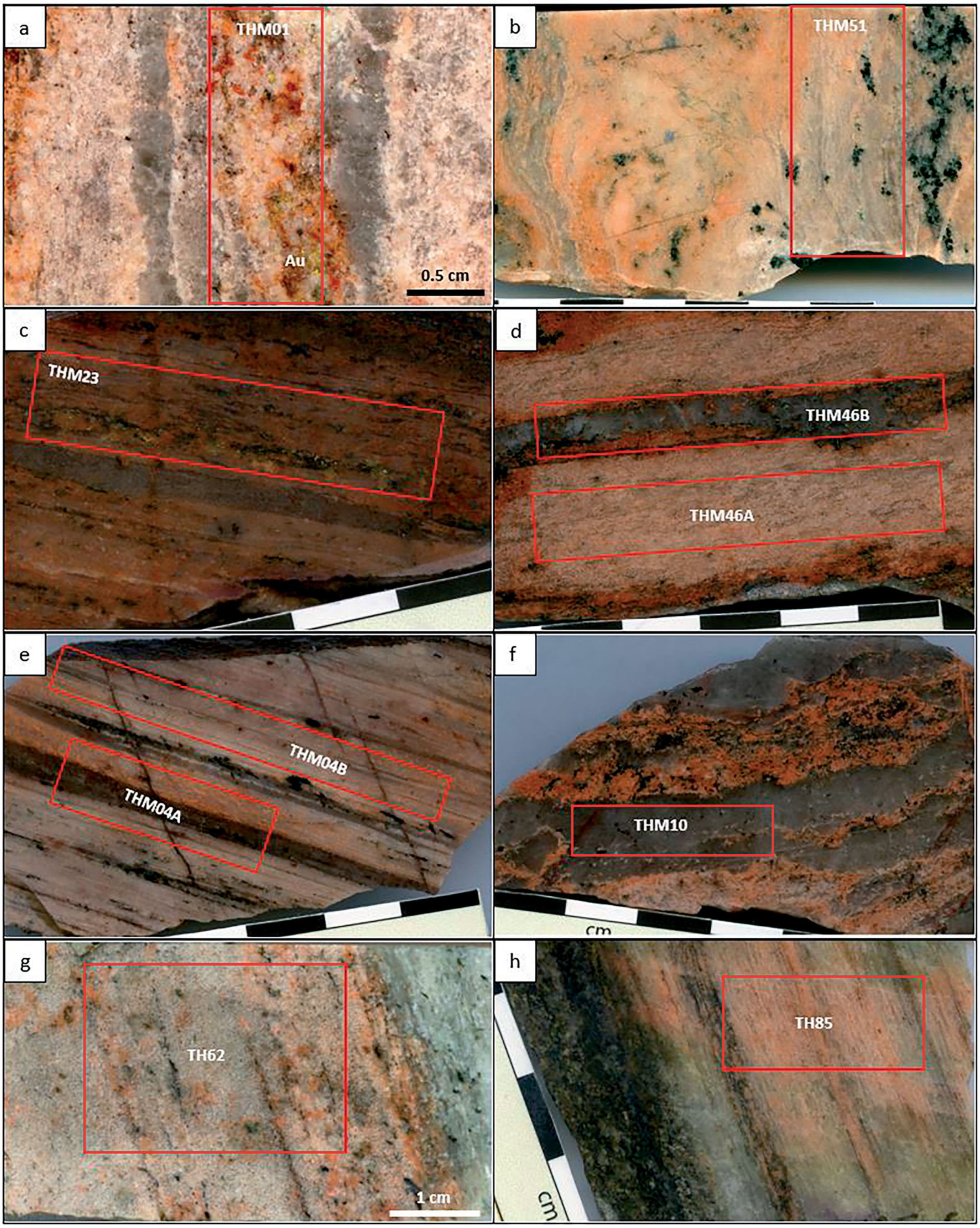

Figure 3. Representative images of quartz–feldspar samples selected for the oxygen isotope analysis. Site of analysis marked by red boxes: (a–f) quartz–feldspar alteration, including Au-rich quartz–feldspar laminae and laminated quartz veins; and (g–h) non-Au-bearing quartz–feldspar alteration overprinting silicified units.

veins and D_3 pegmatites range from 10.5 to 12.5‰ ($n = 6$, average value of 12.0 ± 0.7‰) and are similar to the $\delta^{18}O_{quartz}$ values of the host lithology, including intensely silicified calcsilicate (12.2–13.1‰) and quartz–feldspar mylonite (11.3–13.6‰).

The $\delta^{18}O_{quartz}$ values for hanging-wall and footwall quartzite samples vary from 12.2 to 13.5‰ ($n = 3$), with $\delta^{18}O_{quartz}$ values from the footwall quartzite with sedimentary characteristics slightly more positive than values from the hanging-wall quartzite, which is an intensely silicified

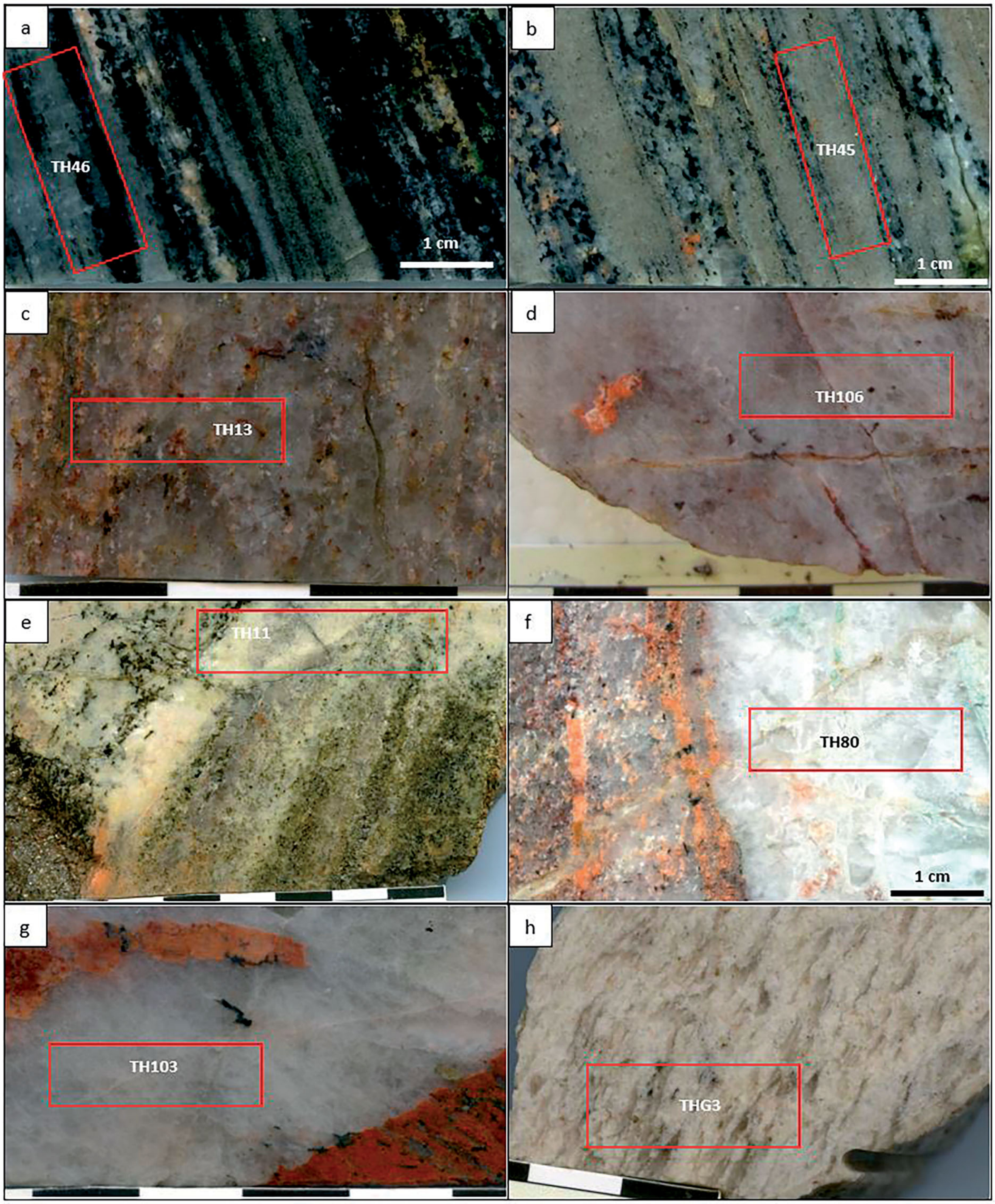

Figure 4. Representative images of different rock units selected for the oxygen isotope analyses. Site of analysis marked by red boxes: (a) intensely silicified amphibole-rich calcsilicate; (b) intensely silicified calcsilicate; (c) metasomatosed quartz–feldspar hanging-wall quartzite; (d) footwall quartzite; (e) D_3 quartz–feldspar veins; (f) D_4 quartz–calcite vein; (g) quartz vein; and (h) syn-D_2 leucogranite.

and quartz–feldspar metasomatised unit (Le *et al.*, 2021a, 2021b). The D_4 quartz–carbonate and quartz veins have $\delta^{18}O_{quartz}$ values of 14.1 and 17.3‰, respectively, *i.e.* 0.4–3.6‰ higher than the upper limit of the general $\delta^{18}O_{quartz}$ range (10.5–13.7‰).

Discussion

Comparison with earlier studies

The new $\delta^{18}O_{quartz}$ results are within error of the earlier results of Choy (1994) and Hannan (1994) (Tables 1–3;

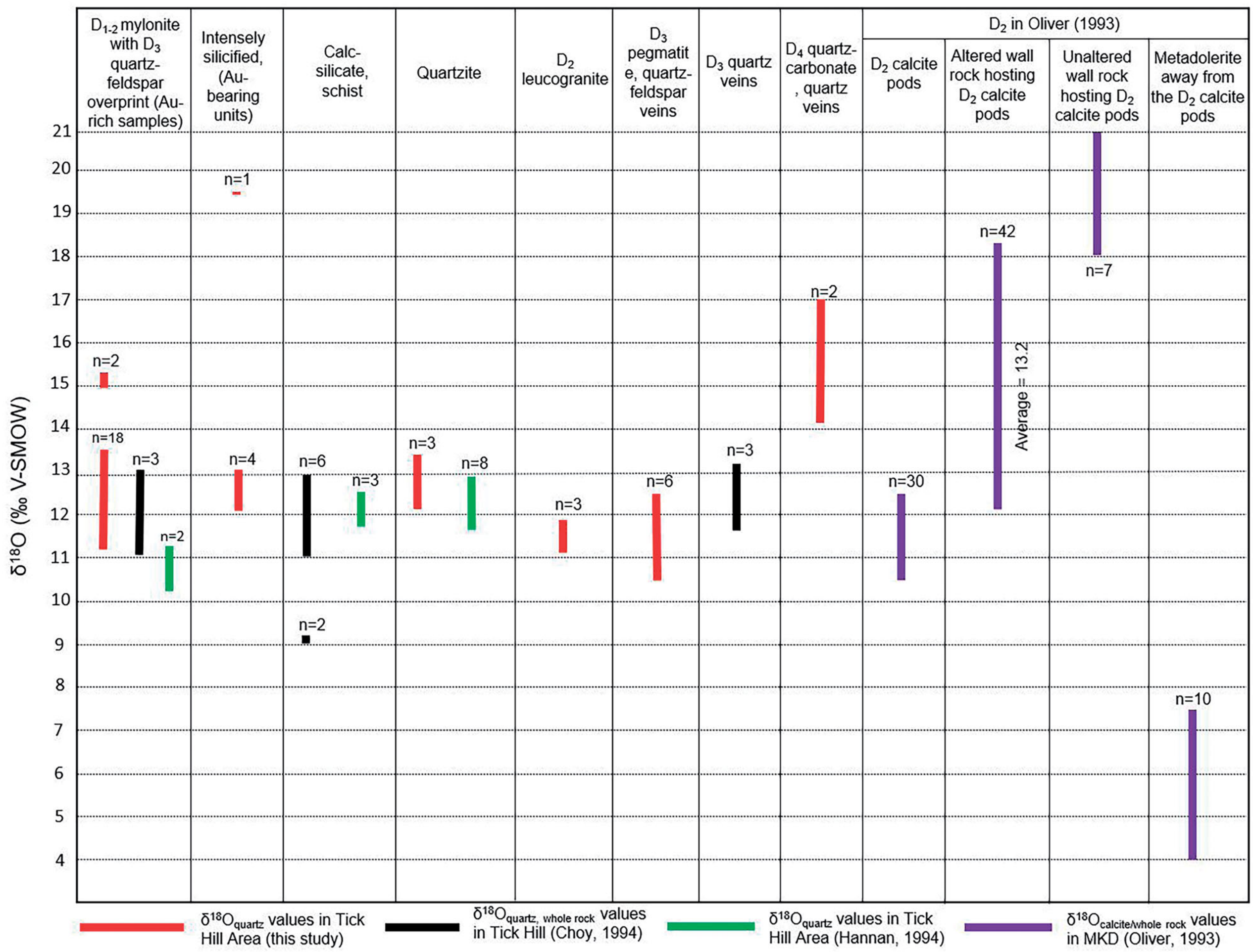

Figure 5. Histogram of all $\delta^{18}O$ values in the Tick Hill area (this study; Choy, 1994; Hannan, 1994) and MKD (Oliver *et al.*, 1993). Note that the D_2 in Oliver *et al.* (1993) equals early D_3 events of this study, whereas D_1 and D_3 in Choy (1994), respectively, equal D_{1-2} and late D_3 of this study.

Figure 5). Results from the mineralised quartz–feldspar mylonite and associated quartz veinlets are relatively homogenous with average $\delta^{18}O_{quartz}$ values of 12.4 ± 0.7‰ (this study; $n = 18$), 10.8‰ ($n = 2$; Hannan, 1994) and 12.3‰ ($n = 3$; Choy, 1994). The depleted $\delta^{18}O_{quartz}$ value (10.3‰; Table 2) for quartzo-feldspathic mylonite mentioned by Hannan (1994) is a single outliner and may reflect the inhomogeneous composition of quartz sampled (*i.e.* ∼5 kg of quartz was crushed for the analysis; Hannan, 1994).

Results from altered, amphibole-bearing calcsilicate in the immediate hanging wall to the ore zone are also similar to earlier results with averages of 12.5 ± 0.4‰ ($n = 4$; this study) and 12.3 ± 0.7‰ ($n = 6$; Choy, 1994), and are within error of the values for the mineralised quartz–feldspar mylonite.

Are the highly mineralised zones characterised by a specific $\delta^{18}O_{quartz}$ values?

The $\delta^{18}O_{quartz}$ values (Tables 1–3) from the highly mineralised and altered quartz–feldspar mylonite are indistinguishable from the highly altered hanging-wall calcsilicate and quartzite units. The $\delta^{18}O_{quartz}$ values for mineralised mylonite and leucogranites, which occur 300 m east of Tick Hill (sample THG3) and 4.5 km southwest of the pit (sample THG4), also overlap. These leucogranites are geochemically similar to the mineralised quartz–feldspar mylonite samples (Le *et al.*, 2021b), and are strongly albitised, although they are not as strongly altered as the rocks in the pit.

The $\delta^{18}O_{quartz}$ values from the mineralised zones cannot be distinguished from unmineralised altered rocks. The $\delta^{18}O_{quartz}$ values are similar for a range of different rock types, with little variation both within the pit and more regionally (*cf.* Hannan, 1994) and further confirms the observations of Oliver *et al.* (1993) that the MKD was affected by a widespread pervasive fluid alteration event. During this event, the $\delta^{18}O$ values of most rocks in the MKD were likely re-equilibrated with a voluminous fluid reservoir that infiltrated from depth. This narrow range of $\delta^{18}O$ values is also displayed in calcite deposited during IOCG mineralisation and Na–(Ca) alteration in the Eastern Succession (Marshall & Oliver, 2008), reflecting the large regional extent of fluids affecting the Mount Isa Inlier during D_3 events.

Table 3. $\delta^{18}O_{quartz}$ values from various rock types in and around the Tick Hill deposit.

Group	No.	Sample ID	Rock type	Zone 54-GDA94 DH./*X* (m)	Zone 54-GDA94 Depth (m)/*Y* (m)	Mineral	Description	$\delta^{18}O$‰ V-SMOW
Au-bearing quartz–feldspar mylonite and laminated quartz veins	1	THM01	Quartz–feldspar mylonite	Ore zone, mining pit		Quartz	High-grade, Au-rich quartz–pink feldspar mylonite	12.6
	2	THM04A	Quartz–feldspar mylonite	Ore zone, mining pit		Quartz	Au-rich quartz–feldspar mylonite with thin laminated quartz veins	13.2
	3	THM04B	Quartz vein inside quartz–feldspar mylonite	Ore zone, mining pit		Quartz	Thin quartz vein (2–3 mm); quartz grains are laminated	13.2
	4	THM10	Quartz vein inside quartz–feldspar alteration zone	Ore zone, mining pit		Quartz	Au-bearing thin quartz vein (1.2 cm wide)	12.6
	5	THM23	Quartz–feldspar mylonite	Ore zone, mining pit		Quartz	1.5 cm wide band of Au-rich quartz–red-pink feldspar	12.4
	6	THM24	Quartz–feldspar mylonite	Ore zone, mining pit		Quartz	0.8 cm wide band of Au-rich quartz–red-pink feldspar	13.4
	7	THM26	Quartz–feldspar mylonite	Ore zone, mining pit		Quartz	1.3 cm Au-rich quartz–red-pink feldspar bands intercalated with laminar quartz veins	11.5
	8	THM40	Quartz–feldspar mylonite	Ore zone, mining pit		Quartz	Au-rich quartz–light pink feldspar mylonite	13.6
	9	THM46A	Quartz–feldspar mylonite	Ore zone, mining pit		Quartz	1 cm wide band of Au-rich quartz–feldspar mylonite with thin laminated quartz veins	12.5
	10	THM46B	Quartz vein inside quartz–feldspar mylonite	Ore zone, mining pit		Quartz	Thin quartz vein intercalated with Au-bearing quartz–feldspar mylonite	11.7
	11	THM51	Quartz–feldspar mylonite	Ore zone, mining pit		Quartz	Au-rich quartz–light pink feldspar–amphibole mylonite	11.3
	12	THM56A	Quartz–feldspar mylonite	Ore zone, mining pit		Quartz	2.5 cm wide band of Au-rich quartz–feldspar laminate (overprinted by red rock alteration)	12.0
	13	THM56B	Quartz vein inside quartz–feldspar mylonite	Ore zone, mining pit		Quartz	0.8 cm wide quartz veins next to Au-rich band	12.7
	14	TH48	Quartz–feldspar mylonite	DH.U9205	54.15	Quartz	Au-rich quartz–bright feldspar mylonite with laminated quartz grains	15.2
	15	TH51	Quartz–feldspar mylonite	DH.U9205	56.4	Quartz	Au-rich quartz–pale pink feldspar mylonite	12.3
	16	TH73	Quartz–feldspar mylonite	DH.TH007	102.3	Quartz	Au-rich quartz–pink feldspar mylonite with micro lenses of quartz and laminated quartz veins with ribbon-like quartz grains	12.4
	17	TH74	Quartz–feldspar mylonite	DH.TH007	106.2	Quartz	Au-rich quartz–pink feldspar mylonite with micro lenses of quartz. Some quartz grains are laminated	12.5
	18	TH105	Quartz–feldspar mylonite	DH.TH014	71.5	Quartz	Au-rich quartz–feldspar mylonite	14.9
Non-Au quartz–feldspar	19	TH62	Quartz–feldspar altered mylonite	DH.U9205	76.8	Quartz	1 cm wide, D_3-stage 2 quartz–feldspar vein overprinted by D_3-stage 3 alteration; no gold	11.9
	20	TH85	Quartz–feldspar altered mylonite	DH.U8506	180.5	Quartz	D_3 pale pink feldspar veins truncating mylonitic quartzite causing quartz–feldspar alteration haloes. Similar to $D_{1/2}$ quartz–feldspar mylonite	12.8
Intensely silicified units	21	TH45	Calc-silicate gneiss	DH.U9205	53.1	Quartz	Intensely silicified calcsilicate	19.4
	22	TH46	Amphibole-rich calcsilicate gneiss	DH.U9205	54.05	Quartz	Intensely silicified Au-bearing amphibole-rich calcsilicate, most quartz grains are equant (annealed)	13.1
	23	TH56	Amphibole-rich calcsilicate gneiss	DH.U9205	59.85	Quartz	Intensely silicified amphibole-rich calcsilicate, most quartz grains are equant (annealed)	12.2
	24	TH60	Amphibole-rich calcsilicate gneiss	DH.U9205	62.8	Quartz	Silicified quartz amphibolite, most of quartz grains are ribbon-like, with pyrite and chalcopyrite	12.3
	25	TH61	Amphibole-rich calcsilicate	DH.U9205	73.4	Quartz	Silicified coarse-grained quartz, overprinting an older fabric defined by amphiboles	12.3
D_3 pegmatite dykes and quartz–feldspar veins	26	TH65	D_3 pegmatite dyke (1525–1520 Ma)	DH.U9205	144.75	Quartz	Coarse quartz grains, with undulose extinction	12.5
	27	TH68	D_3 quartz–feldspar vein	DH.TH007	64.95	Quartz	D_3-stage 1 quartz–feldspar veins overprinted by D_3-stage 3 (quartz–feldspar and hematite–chlorite–epidote alteration) (D_3 *ca* 1522 Ma)	10.5

(*Continued*)

Table 3. (*Continued*).

Group	No.	Sample ID	Rock type	Zone 54-GDA94 DH./*X* (m)	Depth (m)/*Y* (m)	Mineral	Description	$\delta^{18}O$‰ V-SMOW
	28	TH84	D_3 pegmatite dyke (1525–1520 Ma)	DH.U8506	141.5	Quartz	Pegmatite with coarse-grained biotite, coarse-grained quartz and red-pink feldspar	11.9
	29	TH87	D_3 pegmatite dyke (1525–1520 Ma)	DH.U8506	144.1	Quartz	Coarse quartz grains, with undulose extinction	12.3
	30	TH97	D_3 quartz–feldspar vein into amphibolite	DH.DJ525	299	Quartz	Coarse grains of quartz–pink feldspar overprint amphibolite; pure quartz was picked	11.8
	31	TH11	D_3 pegmatite dyke (1525–1520 Ma)	388869	7605868	Quartz	Coarse quartz grains, with undulose extinction	12.2
D_4 veins	32	TH80	D_4 quartz–carbonate vein	DH.TH007	137	Quartz	D_4-stage 6 vein—latest vein (quartz–carbonate–clay minerals)	14.1
	33	TH103	D_4 quartz vein	DH.UG1	209.2	Quartz	D_4 clean quartz vein	17.0
Quartzite	34	TH104	Hanging wall quartzite	DH.TH014	61	Quartz	Coarse-grained quartz, overprinting an older foliated fabric defined by scattered and altered feldspars that give the rock a speckled appearance	12.2
	35	TH106	Foot wall quartzite	DH.TH014	85.5	Quartz	Coarse-grained quartz; strongly recrystallised and annealed with few inclusions	13.5
	36	TH13	Hanging wall quartzite	388842	7605827	Quartz	Coarse-grained quartz, overprinting an older foliated fabric defined by scattered and altered feldspars	13.0
D_2 leucogranite	37	THM32	D_2 leucogranite	Tick Hill Area		Quartz	Quartz–white to pale pink feldspar mylonite without Au; contains laminated quartz grains	11.8
	38	THG3	D_2 leucogranite (*ca* 1777 Ma)	389258	7605939	Quartz	Ribbon quartz in gneissic layering	11.2
	39	THG4	D_2 leucogranite (*ca* 1777 Ma)	386702	7603938	Quartz	Ribbon quartz in gneissic layering	11.8

Some of the quartz–feldspar mylonite samples and one of the altered calcsilicate samples as well as the footwall quartzite have enriched $\delta^{18}O_{quartz}$ values. These may represent analytical errors considering the homogenous nature of results from all other samples that are similar in composition, deformation style and alteration assemblage. Alternatively, it has been noted that regional background $\delta^{18}O_{quartz}$ values are enriched to 17–21‰ within the calcsilicates of the Corella Formation (*e.g.* Oliver, 1995; Oliver *et al.*, 1993). The elevated values obtained in this study (Table 3) could, therefore, reflect primary $\delta^{18}O_{quartz}$ values or enrichment during metamorphism owing to decarbonation reactions that have been only partly re-equilibrated by a later fluid during regional alteration.

Do similar rock types of different ages have different $\delta^{18}O_{quartz}$ values?

Choy (1994) showed the $\delta^{18}O_{quartz}$ values from syn-D_1 (peak-metamorphic gneissic fabric) and syn-D_3 (later alteration overprint, including red rock alteration) quartz were statistically indistinguishable. Most $\delta^{18}O_{quartz}$ values fall within a narrow range (10.5–13.7‰) with no significant and systematic differences between different rock types or between mineralised and non-mineralised samples. Results from samples containing the pervasive D_{1-2} fabric, estimated to have formed around 1780 Ma (Le *et al.*, 2021b) and affected by retrogression and younger alteration, are indistinguishable from samples obtained from later quartz–feldspar veins and pegmatites (with a $\delta^{18}O_{quartz}$ value of 12.0 ± 0.7‰) that were dated at 1525–1520 Ma (Le *et al.*, 2021b).

Therefore, the $\delta^{18}O_{quartz}$ values were affected by deformation–metamorphism–alteration between D_1 and D_3 and are indistinguishable from one another, which is consistent with observations made by Oliver *et al.* (1993). The various fluid pulses affecting the rocks during D_1, D_2 and D_3 either all had similar isotope values, or that the rocks were affected by a pervasive hydrothermal alteration during D_3, which resulted in resetting the $\delta^{18}O_{quartz}$ values in all rock types throughout the region. The latter interpretation is consistent with similar conclusions in previous studies (*e.g.* Mark *et al.*, 2006; Oliver, 1995; Oliver *et al.*, 1993; Williams *et al.*, 2005; Withnall & Hutton, 2013).

Two samples obtained from later D_4 fault-related quartz–calcite cataclastic veins yield elevated $\delta^{18}O_{quartz}$ values of 14.1 and 17.0‰, which are distinctly higher than the older quartz and may reflect: (1) the fluid sourced from metamorphic water (Rollinson, 1993) that locally overprinted the pervasive alteration; (2) the breakdown of carbonate from host detrital sediments into fluids (Rollinson, 1993) during the D_4 events; or (3) fluids that was possibly resulted from the partial re-equilibration of minerals in the cataclastic fault rocks during D_4 events. The first interpretation, however, is not likely because the D_4 events have not been aligned with any regional metamorphic event.

Possible fluid sources for the Au-bearing quartz?

Based on near uniform $\delta^{18}O_{calcite}$ results for calcite pods along the length of the MKD, Oliver (1995) and Oliver *et al*. (1993) argued for a single homogenous, high-volume fluid reservoir that pervasively reset oxygen isotope values in the host rocks. With the poorly constrained genetic relationship between the metamorphic event and granitic magmatism, an intrusive source in either the lower crust or upper mantle was considered more likely than locally derived metamorphic fluids. This fluid event was assumed to have occurred during the Isan Orogeny at *ca* 1550 Ma.

Spence *et al*. (2021), who remapped parts of the area reported by Oliver *et al*. (1993), showed that upright folding and peak metamorphism was diachronous across the area; before 1715 Ma in the Mt Godkin area and before 1735 Ma in the Mary Kathleen–Duchess area. This implies that if the field relationships for the calcite pods described by Oliver *et al*. (1993) were correct, carbonate vein emplacement and associated chalcopyrite enrichment would have occurred before 1715 Ma. Spence *et al*. (2021) further noted that the timing of Isan Orogeny events within the MKD, appear to be largely constrained to networks of shear zones that reactivated earlier fabrics, with renewed amphibolite facies metamorphism and extensive alteration. Our field observations for several calcite pods described by Oliver *et al*. (1993) indicate that calcite grains in these veins are extremely coarse-grained and recrystallised, despite the strongly deformed nature of the pods, indicating post-deformational annealing. This could mean that the metamorphic conditions of emplacement (530–570 °C) based on calcite–dolomite geothermometry reported by Oliver *et al*. (1993) do not record peak-metamorphic conditions during upright folding at >1715 Ma, but rather record the elevated temperatures attained during recrystallisation/annealing by a regionally pervasive hydrothermal fluid during the Isan Orogeny.

The existence of a late Isan hydrothermal overprint is confirmed by widely reported 1525–1520 Ma ages for hydrothermal titanite and high-U zircon overgrowths along the length of the MKD (*e.g.* Bodorkos *et al*., 2020; Kositcin *et al*., 2019; Withnall, 2019). At Tick Hill, this same event has been recorded in the emplacement of quartz–feldspar veins, pegmatite dykes, extensive alteration and gold mineralisation (Le, 2021). Thus, the $\delta^{18}O_{quartz}$ results from the Tick Hill area reported here (10.5–13.7‰) most likely reflect fluid conditions (380–550 °C; Le, 2021) at 1525–1520 Ma, during the late Isan hydrothermal overprint.

Given the well-documented regional extent of the late Isan overprint across the EFB (*e.g.* Oliver *et al*., 2008), we can assume that the $\delta^{18}O_{calcite}$ values reported for the MKD by Oliver *et al*. (1993) and the $\delta^{18}O_{quartz}$ results reported here for Tick Hill, reflect the same hydrothermal overprint. If we further assume that the uniform $\delta^{18}O_{calcite}$ values along a 100 km stretch between Mt Godkin and Trekalano Mine, are also at Tick Hill, 18 km south of the Trekelano Mine, then the reported average $\delta^{18}O_{calcite}$ and $\delta^{18}O_{quartz}$ values can be used to estimate the temperature of the late Isan hydrothermal fluid reservoir. However, the $\delta^{18}O_{calcite}$ and $\delta^{18}O_{quartz}$ values used for geochronology were not from the same samples so the calculation and should be used with caution in making temperature estimates. Annealed quartz grains associated with gold and D_3 alteration assemblages from mineralised quartz–feldspar mylonite are estimated to have formed between 380–550 °C (Le, 2021).

Using geothermometers based on the fractionation of oxygen isotopes in mineral pairs that co-precipitated from the same hydrothermal fluid (Faure, 1986; Friedman & O'Neil, 1977; Matthews *et al*., 1983) and assuming an average value for $\delta^{18}O_{calcite}$ of 10.73 ± 0.39‰ ($n = 10$) from retrograde calcite pods (Oliver *et al*., 1993), and an average $\delta^{18}O_{quartz}$ value of 12.43 ± 0.66‰ from mineralised quartz–feldspar mylonite data presented here, a fluid temperature of 321 °C is calculated. If the data reported in Choy (1994) and Hannan (1994) are included (average $\delta^{18}O_{quartz}$ of 12.2‰) this increases to 366 °C. Combining this average $\delta^{18}O_{quartz}$ value with the average $\delta^{18}O_{calcite}$ value of 11.54 ± 0.67‰ ($n = 20$) for the high-temperature calcite pods (Oliver *et al*., 1993) provides a temperature estimate of 548 °C. While these temperature estimates are dependent on many assumptions, the difference in $\delta^{18}O_{quartz}$ and $\delta^{18}O_{calcite}$ values is consistent with equilibrium at high temperatures and with the observed early stage, upper-greenschist facies D_3 alteration assemblages at Tick Hill (hornblende–albite–quartz–magnetite and actinolite–chlorite–epidote assemblages; Le, 2021; Le *et al*., 2021a). Thus, the $\delta^{18}O_{quartz}$ results for quartz in Tick Hill appear to reflect the earlier stages of fluid infiltration at 1525–1520 Ma, before and during the main-stage of gold mobilisation.

The precipitation of various Bi-selenides and low temperature (130–170 °C) of chlorite during late-stage gold mobilisation (Le *et al*., 2021a) suggests lithostatic pressures below 1 kbar and the veins and host rocks were relatively close to surface (Le *et al*., 2021a; Simon *et al*., 1997). The late D_3 events at Tick Hill are linked to the regional Isan Orogeny (Le *et al*., 2021b); hence the geothermal gradients at Tick Hill would have been high across large areas.

The origin of the hydrothermal fluids is unclear, and the $\delta^{18}O_{quartz}$ values do not provide a conclusive answer, as they overlap with reported $\delta^{18}O$ values for both metamorphic and igneous fluids (*e.g.* Blatt, 1987; Harris & Vogeli, 2010; Rollinson, 1993). An igneous source is commonly invoked (*e.g.* Oliver *et al*., 2008), involving the laterally extensive upper- to mid-crustal granites of the Williams-Naraku Batholith (*e.g.* Mark, 2001; Oliver *et al*., 2008; Page & Sun, 1998), in combination with a CO_2-rich fluid component released from mafic rocks in the lower crust or mantle (Oliver *et al*., 2008). At Tick Hill, there is no direct evidence for late-tectonic intrusions (or CO_2-rich fluids) other than the 1525–1520 Ma pegmatite veins.

Conclusions

At Tick Hill, the $\delta^{18}O_{quartz}$ values for Au-rich host units, including quartz–feldspar mylonite and intensely silicified schist and quartzite, vary from 11.3% to 13.6‰ are similar to the $\delta^{18}O_{quartz}$ values from surrounding rock types. The results from this study, like those from earlier $\delta^{18}O_{quartz}$ studies conducted at Tick Hill and the surrounding areas, do not provide a useful exploration tool proposed by Hannan (1994).

The $\delta^{18}O_{quartz}$ results from the Tick Hill area reflect widespread fluid infiltration that re-equilibrated minerals, especially quartz in the MKD, during the late Isan hydrothermal overprint at 1525–1520 Ma. The origin of the hydrothermal fluids is unclear, and the $\delta^{18}O_{quartz}$ values do not provide a conclusive answer. Combining the $\delta^{18}O_{quartz}$ results with published $\delta^{18}O_{calcite}$ results gives temperature estimates that are consistent with the 380–550 °C temperatures suggested for the albite–amphibole alteration assemblages during early D_3 events. The D_4 quartz–calcite veins that postdate the 1525–1520 Ma D_3 deformation and mineralisation events have higher $\delta^{18}O_{quartz}$ values, 14.1–17‰, possibly related to the (partial) re-equilibration of minerals in the cataclastic fault rocks during D_4 events as well as the breakdown of carbonate from the host rock into the D_4 veins.

Acknowledgements

We would like to thank the Geological Survey of Queensland, the Economic Geology Research Centre (EGRU, James Cook University) and Rick Valenta who set up the Tick Hill Study Project. We would like to thank Peter Rea, Alex Brown from Glencore, Mount Isa Mines and Paul Tan, Brett Davis and Rob Watkins from Carnaby Resources for providing logistic support for fieldwork, access to drill core and data sets. Our thanks to Nick Oliver for donating Tick Hill samples and numerous discussions.

Disclosure statement

No potential conflict of interest was reported by the author(s)

Funding

Funding for this study was provided by the Department of Natural Resources, Mines and Energy.

ORCID

T. X. Le http://orcid.org/0000-0001-8137-1134
J. M. Huizenga http://orcid.org/0000-0003-3254-702X

Data availability statement

The oxygen isotope data of Choy (1994) for the Tick Hill deposit that support the findings of this study are available at the Hargrave-Andrew Library in Monash University in the form of hard copy and film. The oxygen isotope data of Hannan (1994) for the Tick Hill area that support the findings of this study are available at the Mount Isa Mine Exploration office and are available with permission.

References

Abu Sharib, A. S. A. A., & Sanislav, I. V. (2013). Polymetamorphism accompanied switching in horizontal shortening during Isan Orogeny: example from the Eastern Fold Belt, Mount Isa Inlier, Australia. *Tectonophysics*, *587*, 146–167. https://doi.org/10.1016/j.tecto.2012.06.051

Betts, P., Giles, D., Mark, G., Lister, G., Goleby, B., & Ailleres, L. (2006). Synthesis of the Proterozoic evolution of the Mt Isa Inlier. *Australian Journal of Earth Sciences*, *53*(1), 187–211. https://doi.org/10.1080/08120090500434625

Blake, D. H. (1987). Geology of the Mt Isa inlier and environs, Queensland and Northern Territory. Australian Bureau of Mineral Resources, *Geology and Geophysics, Bulletin*, *225*, 1–83.

Blake, D., & Steward, A. (1992). Stratigraphic and tectonic framework, Mt Isa. *AGSO Bulletin*, *243*, 1–11.

Blatt, H. (1987). Perspectives; Oxygen isotopes and the origin of quartz. *Journal of Sedimentary Research*, *57*(2), 373–377. https://doi.org/10.1306/212F8B34-2B24-11D7-8648000102C1865D

Boda, S. (1994). Sample list, description, locations of samples for quartz isolation and $\delta^{18}O$ analysis. *MIMEX Memorandum to K. Hannan 27 Jun 1994*, file code TH5.2, 9pp, Mt Isa exploration office.

Bodorkos, S., Purdy, D. J., Bultitude, R. J., Lewis, C. J., Jones, S. L., Brown, D. D., & Hoy, D. (2020). Summary of Results. In *Joint GSQ-GA Geochronology Project: Mary Kathleen Domain and Environs, Mt Isa Inlier, 2018–2020. Queensland Geological Record 2020/04.*

Choy, D. K. W. (1994). *The geology, structure, petrology, alteration and mineralisation of Tick Hill, North-West Queensland* [Unpublished Master Thesis]. Monash University.

Faure, G. (1986). *Principles of Isotope Geology*. Wiley.

Foster, D. R. W., & Rubenach, M. J. (2006). Isograd pattern and regional low-pressure, high-temperature metamorphism of pelitic, mafic and calc-silicate rocks along an east–west section through the Mt. Isa Inlier. *Australian Journal of Earth Sciences*, *53*(1), 167–186. https://doi.org/10.1080/08120090500434617

Foster, D. R., & Austin, J. R. (2008). The 1800–1610 Ma stratigraphic and magmatic history of the Eastern Succession, Mt Isa Inlier, and correlations with adjacent Paleoproterozoic terranes. *Precambrian Research*, *163*(1–2), 7–30. https://doi.org/10.1016/j.precamres.2007.08.010

Friedman, I., & O'Neil, J. R. (1977). *Compilation of stable isotope fractionation factors of geochemical interest*. US Geological Survey Professional Paper, 440-KK. https://doi.org/10.3133/pp440KK

Gibson, G. M., Meixner, A. J., Withnall, I. W., Korsch, R. J., Hutton, L. J., Jones, L. E. A., Holzschuh, J., Costelloe, R. D., Henson, P. A., & Saygin, E. (2016). Basin architecture and evolution in the Mount Isa mineral province, northern Australia: constraints from deep seismic reflection profiling and implications for ore genesis. *Ore Geology Reviews*, *76*, 414–441. https://doi.org/10.1016/j.oregeorev.2015.07.013

Giles, D., Betts, P. G., & Lister, G. S. (2002). Far-field continental backarc setting for 1.80–1.67 Ga basins of northern Australia. *Geology*, *30*(9), 823–826. https://doi.org/10.1130/0091-7613(2002)030<0823:FFCBSF>2.0.CO;2

Hannan, K. (1994). Tick Hill District quartz oxygen isotope results. *Report to MIM Exploration Pty Ltd*, Memo.1996/024, Record No. 18742, Mt Isa exploration office.

Harris, C., & Vogeli, J. (2010). Oxygen isotope composition of garnet in the Peninsula Granite, Cape Granite Suite, South Africa: Constraints on melting and emplacement mechanisms. *South African Journal of Geology*, *113*(4), 401–396. https://doi.org/10.2113/gssajg.113.4.401

Holcombe, R., Pearson, P., & Oliver, N. (1991). Geometry of a middle Proterozoic extensional decollement in northeastern Australia.

Tectonophysics, *191*(3–4), 255–274. https://doi.org/10.1016/0040-1951(91)90061-V

Kleine, B. I., Stefansson, A., Halldórsson, S. A., Whitehouse, M. J., & Jónasson, K. (2018). Silicon and oxygen isotopes unravel quartz formation processes in the Icelandic crust. *Geochemical Perspectives Letters*, *7*, 5–11. https://doi.org/10.7185/geochemlet.1811

Kositcin, N., Bultitude, R. J., & Purdy, D. J. (2019). Queensland Geological Record 2019/02. Summary of results. In *Joint GSQ-GA Geochronology Project: Mary Kathleen Domain, Mt Isa Inlier, 2018–2019*. Queensland Geological Record 2019/02.

Le, T. X. (2021). *Geological characteristics, genesis and ore controlling factors of the Tick Hill Au deposit, Dajarra District, NW Queensland, Australia* [Unpublished PhD thesis]. James Cook University.

Le, T. X., Dirks, P. H. G. M., Sanislav, I. V., Huizenga, J. M., Cocker, H., & Manestar, G. N. (2021a). Geological setting and mineralization characteristics of the Tick Hill Gold Deposit, Mt Isa Inlier, Queensland, Australia. *Ore Geology Reviews*, *137*, 104288. https://doi.org/10.1016/j.oregeorev.2021.104288

Le, T. X., Dirks, P. H. G. M., Sanislav, I. V., Huizenga, J. M., Cocker, H., & Manestar, G. N. (2021b). Geochronological constraints on the geological history and gold mineralisation in the Tick Hill region, Mt Isa Inlier. *Precambrian Research*, *366*, 106422. https://doi.org/10.1016/j.precamres.2021.106422

MacCready, T., Goleby, B. R., Goncharov, A., Drummond, B. J., & Lister, G. S. (2006). Shifts in the locus of crustal thickening during mesoproterozoic orogenesis in the Mt Isa Terrane. *Australian Journal of Earth Sciences*, *53*(1), 41–53. https://doi.org/10.1080/08120090500432405

Mark, G. (2001). Nd isotope and petrogenetic constraints for the origin of the Mount Angelay igneous complex: Implications for the origin of intrusions in the Cloncurry district, NE Australia. *Precambrian Research*, *105*(1), 17–35. https://doi.org/10.1016/S0301-9268(00)00101-7

Mark, G., Oliver, N. H., & Williams, P. J. (2006). Mineralogical and chemical evolution of the Ernest Henry Fe oxide–Cu–Au ore system, Cloncurry district, northwest Queensland, Australia. *Mineralium Deposita*, *40*(8), 769–801. https://doi.org/10.1007/s00126-005-0009-7

Marshall, L. J., & Oliver, N. H. (2008). Constraints on hydrothermal fluid pathways within Mary Kathleen Group stratigraphy of the Cloncurry iron-oxide–copper–gold District, Australia. *Precambrian Research*, *163*(1–2), 151–158. https://doi.org/10.1016/j.precamres.2007.08.016

Matthews, A., Goldsmith, J. R., & Clayton, R. N. (1983). Oxygen isotope fractionations involving pyroxenes: the calibration of mineral-pair geothermometers. *Geochimica et Cosmochimica Acta*, *47*(3), 631–644. https://doi.org/10.1016/0016-7037(83)90284-3

Neumann, N., Gibson, G., & Southgate, P. (2009). New SHRIMP age constraints on the timing and duration of magmatism and sedimentation in the Mary Kathleen Fold Belt, Mt Isa Inlier, Australia. *Australian Journal of Earth Sciences*, *56*(7), 965–983. https://doi.org/10.1080/08120090903005410

Oliver, N. H. S. (1995). Hydrothermal history of the Mary Kathleen Fold Belt, Mt Isa Block, Queensland. *Australian Journal of Earth Sciences*, *42*(3), 267–279. https://doi.org/10.1080/08120099508728201

Oliver, N. H. S., Butera, K. M., Rubenach, M. J., Marshall, L. J., Cleverley, J. S., Mark, G., Tullemans, F., & Esser, D. (2008). The protracted hydrothermal evolution of the Mount Isa Eastern Succession: A review and tectonic implications. *Precambrian Research*, *163*(1–2), 108–130. https://doi.org/10.1016/j.precamres.2007.08.019

Oliver, N., Cartwright, I., Wall, V., & Golding, S. (1993). The stable isotope signature of kilometer-scale fracture dominated metamorphic fluid pathways, Mary Kathleen. *Journal of Metamorphic Geology*, *11*(5), 705–720. https://doi.org/10.1111/j.1525-1314.1993.tb00182.x

Page, R., & Sun, S. S. (1998). Aspects of geochronology and crustal evolution in the Eastern Fold Belt, Mt Isa Inlier. *Australian Journal of Earth Sciences*, *45*(3), 343–361. https://doi.org/10.1080/08120099808728396

Passchier, C., & Williams, P. (1989). Proterozoic extensional deformation in the Mt Isa inlier, Queensland, *Australia*. *Geological Magazine*, *126*(1), 43–53. https://doi.org/10.1017/S0016756800006130

Pollard, P. J., & McNaughton, N. J. (1997). *U–Pb geochronology and Sm/Nd isotope characteristics of Proterozoic intrusive rocks in the Cloncurry district, Mount Isa Inlier, Australia, final report project no. P438*. Australian Minerals Industry Research Association.

Rollinson, H. (1993). *Using geochemical data: Evaluation, presentation, interpretation*. Longman Group UK, 352 pp.

Simon, G., Kesler, S. E., & Essene, E. J. (1997). Phase relations among selenides, sulfides, tellurides, and oxides. II. Applications to selenide-bearing ore deposits. *Economic Geology*, *92*(4), 468–484. https://doi.org/10.2113/gsecongeo.92.4.468

Spence, J., Sanislav, I., & Dirks, P. (2021). 1750–1710 Ma deformation along the eastern margin of the North Australia Craton. *Precambrian Research*, *353*, 106019. https://doi.org/10.1016/j.precamres.2020.106019

Williams, P. J., Barton, M. D., Johnson, D. A., Fontboté, L., De Haller, A., Mark, G., Oliver, N. H., & Marschik, R. (2005). Iron oxide–copper–gold deposits: Geology, space–time distribution, and possible modes of origin. In J. W. Hedenquist, J. F. H. Thompson, R. J. Goldfarb & J. P. Richards (Ed.), *Geology of Queensland Economic Geology100th Anniversary Volume* (pp. 371–405). Society of Economic Geologists. https://doi.org/10.5382/AV100.13

Withnall, I. (2019). Review of SHRIMP zircon ages for the Eastern Succession of the Mount Isa Province and magmatic events in its provenance. *Queensland Minerals and Energy Review*, 182 pp. Geological Survey of Queensland.

Withnall, I., & Hutton, L. (2013). Chapter 2: North Australian Craton. In P. A. Jell (Ed.), *Geology of Queensland* (pp. 23–112). Geological Survey of Queensland.